Metallic Nanoparticles – General Considerations

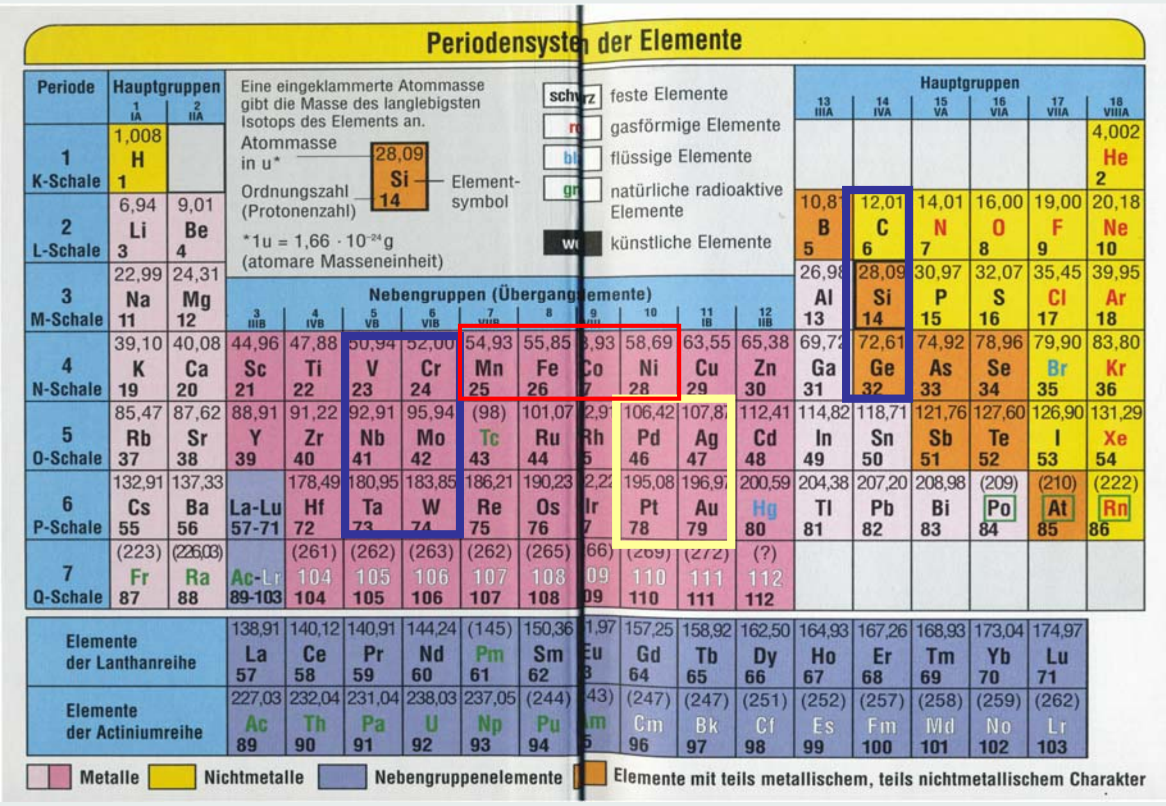

Alkali Metal Clusters Metal Clusters in Chemical Compounds

T. Bergmann, H. Limberger, and T. P. Martin — American Physical Society 1988, VOLUME 60, NUMBER 17, 1767

FIG. 2. Portion of a high-resolution time-of-flight mass spectrum of Cs-O clusters photoionized with 480-nm laser light. The mass peaks of clusters containing two oxygen atoms have been connected.

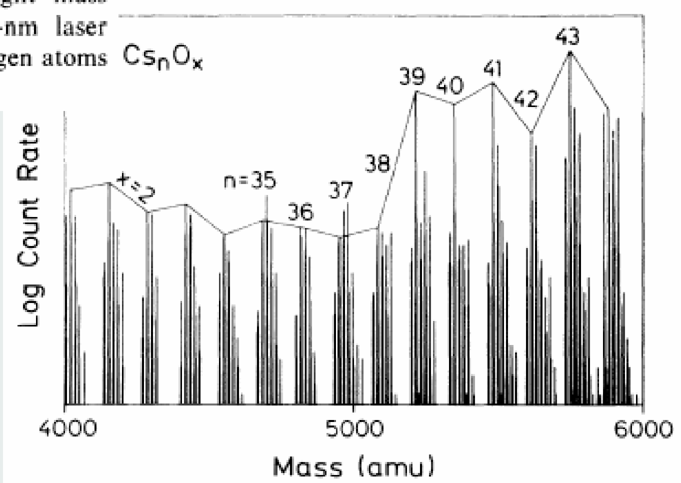

Unusually high ionization energies have been observed for Cs-O clusters having certain sizes and compositions, namely for $Cs_{2n+z}O_n$ with $z = 8$, 18, 34, 58, and 92. The anomalies are well defined for clusters containing from one to seven oxygen atoms. The indicated values of z are identical to the numbers of electrons in closed shells of angular momentum.

From Clusters in Solids to Polymer Clusters

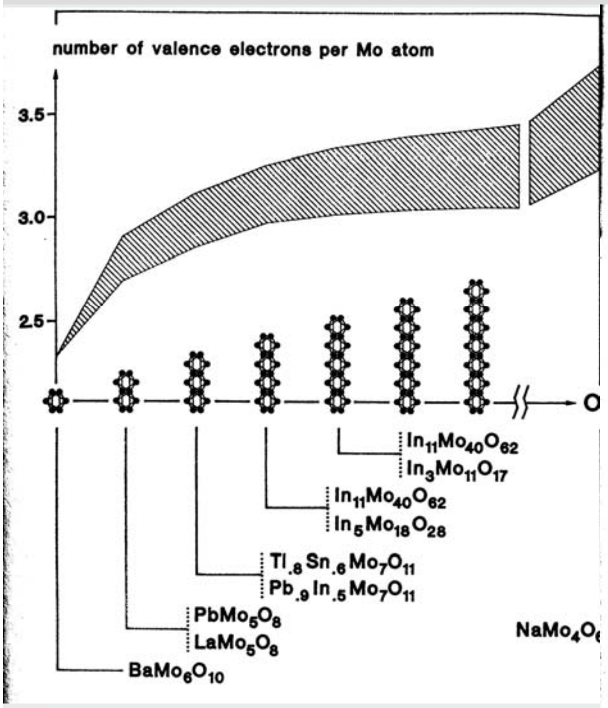

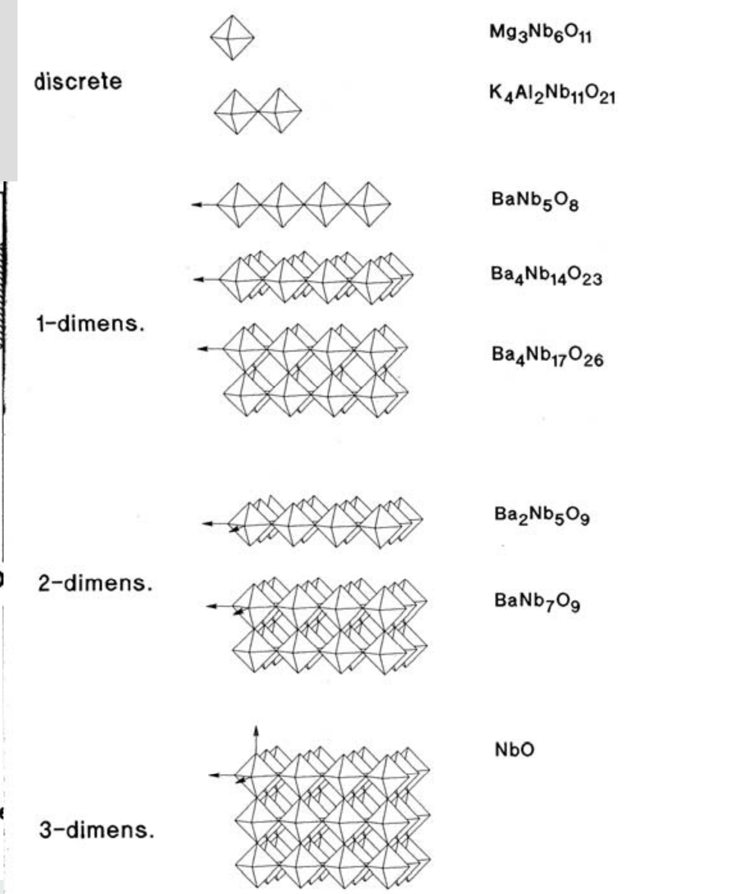

Figure 5-19. Condensed $[Nb_6O_{12}]$ clusters in reduced oxoniobates (schemati[c] octahedra drawn).

Au-Clusters, G. Schmid et al.

Gezielte Synthese von $Au_{55}(PPh_3)_{12}Cl_6$

$[Ph_3PAuCl]$ + B_2H_6 in Toluol

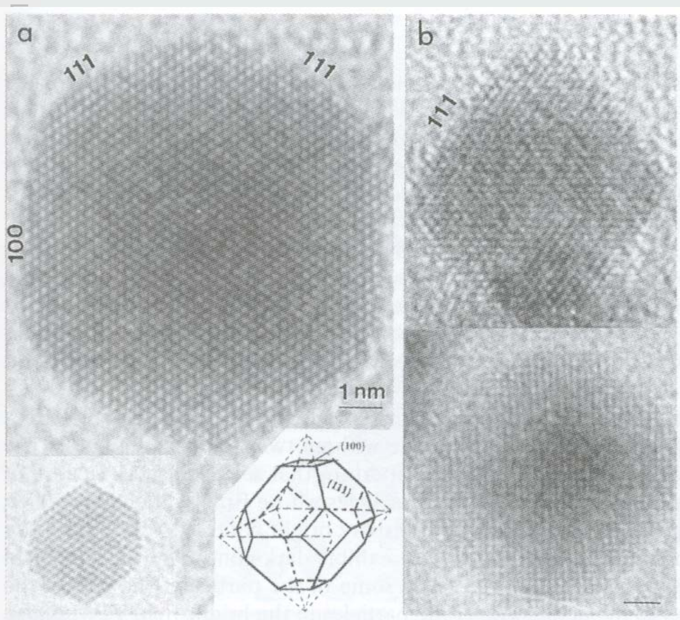

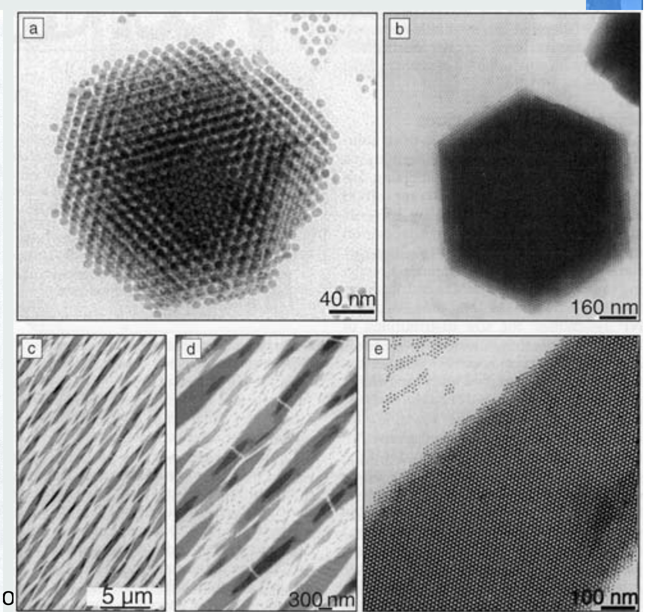

Planar Gold Nanoparticle Clusters as Microscale Mirrors

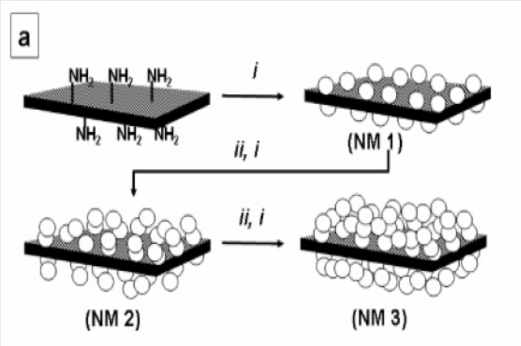

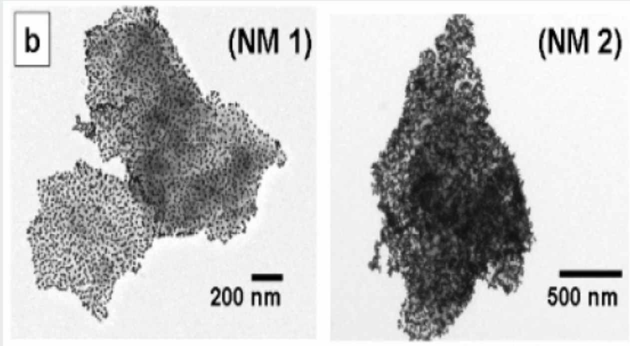

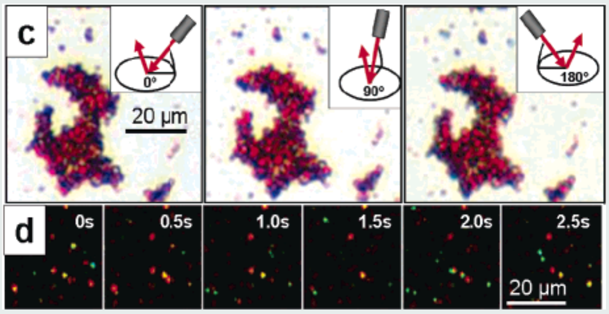

(a) Synthesis of mirror plates. For detailed structure of amine terminated nanoplates, see ref 7. (i) Citrate-coated gold nanoparticles in water:ethanol (1:1 v/v), followed by centrifugation; (ii) 1,8-octanedithiol in ethanol.
(b) Transmission electron micrographs of types **1-3** NMs

J. AM. CHEM. SOC. 2006, 128, 3868-3869

Metallic and Elemental Nanorods

Metals

1 H																	2 He
3 Li	4 Be											5 B	6 C	7 N	8 O	9 F	10 Ne
11 Na	12 Mg											13 Al	14 Si	15 P	16 S	17 Cl	18 Ar
19 K	20 Ca	21 Sc	22 Ti	23 V	24 Cr	25 Mn	26 Fe	27 Co	28 Ni	29 Cu	30 Zn	31 Ga	32 Ge	33 As	34 Se	35 Br	36 Kr
37 Rb	38 Sr	39 Y	40 Zr	41 Nb	42 Mo	43 Tc	44 Ru	45 Rh	46 Pd	47 Ag	48 Cd	49 In	50 Sn	51 Sb	52 Te	53 I	54 Xe
55 Cs	56 Ba		72 Hf	73 Ta	74 W	75 Re	76 Os	77 Ir	78 Pt	79 Au	80 Hg	81 Tl	82 Pb	83 Bi	84 Po	85 At	86 Rn
87 Fr	88 Ra		104 Rf	105 Db	106 Sg	107 Bh	108 Hs	109 Mt	110 Ds	111 Rg	112 Uub	113 Uut	114 Uuq	115 Uup	116 Uuh	117 Uus	118 Uuo

57 La	58 Ce	59 Pr	60 Nd	61 Pm	62 Sm	63 Eu	64 Gd	65 Tb	66 Dy	67 Ho	68 Er	69 Tm	70 Yb	71 Lu
89 Ac	90 Th	91 Pa	92 U	93 Np	94 Pu	95 Am	96 Cm	97 Bk	98 Cf	99 Es	100 Fm	101 Md	102 No	103 Lr

Au-Clusters

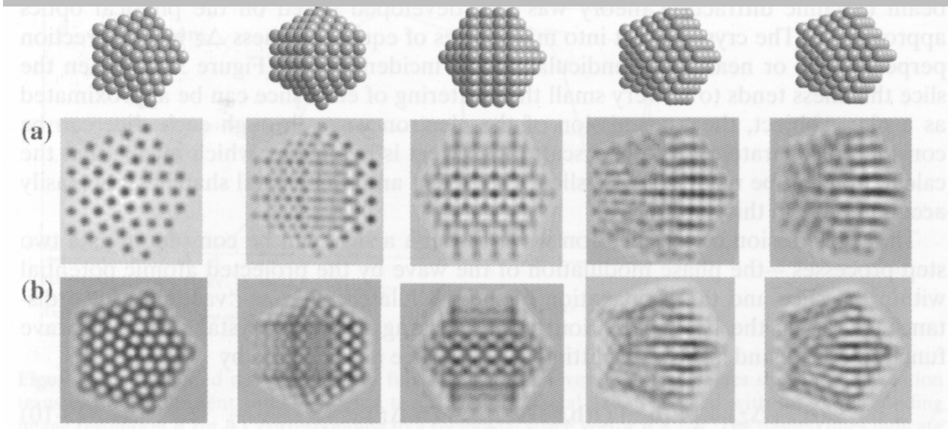

Figure 3-5. Theoretically simulated images for a decahedral Au particle at various orientations and at focuses of (A) $\Delta f = 42$ nm and (B) $\Delta f = 70$ nm. The Fourier transform of the image is also displayed (Courtsey of Drs. Ascencio and M. José-Yacamán).

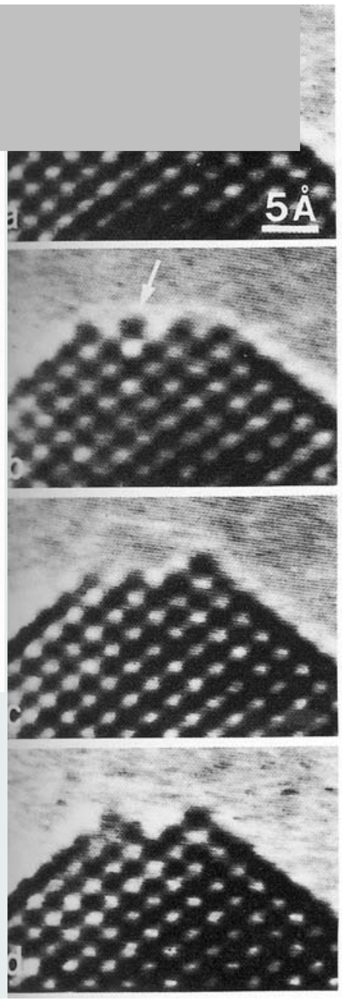

Gold-NPs at different Distances

Figure 5. The transmitted colors of a series of gold particle films with decreasing particle spacing. The gold core particles are 15 nm in diameter; the shell thicknesses are, from left to right, 17.5 nm, 12.5 nm, 4.6 nm, 2.9 nm, 1.5 nm, 1.0 nm, 0.5 nm and 0 nm. Films are each 1 cm × 3 cm. The spectra shift smoothly between the two curves shown in Figure 3 as the spacing is varied.[9]

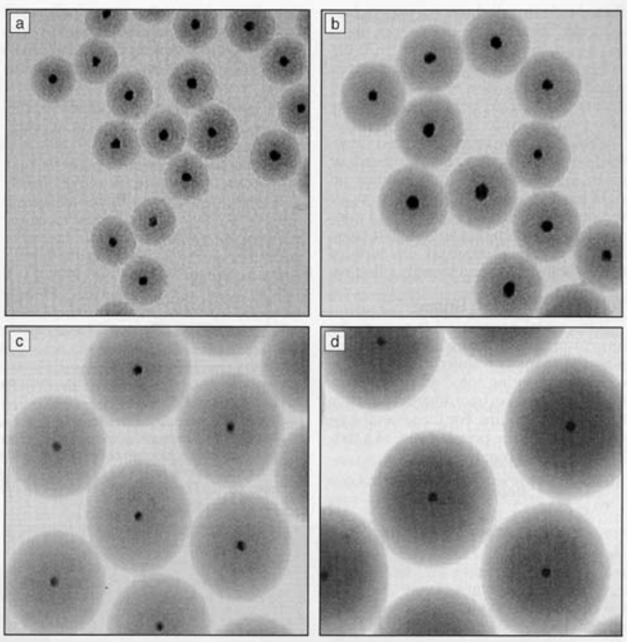

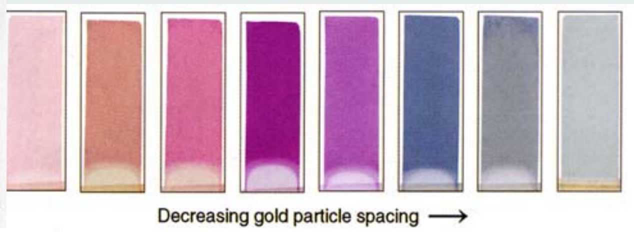

Pd-Clusters

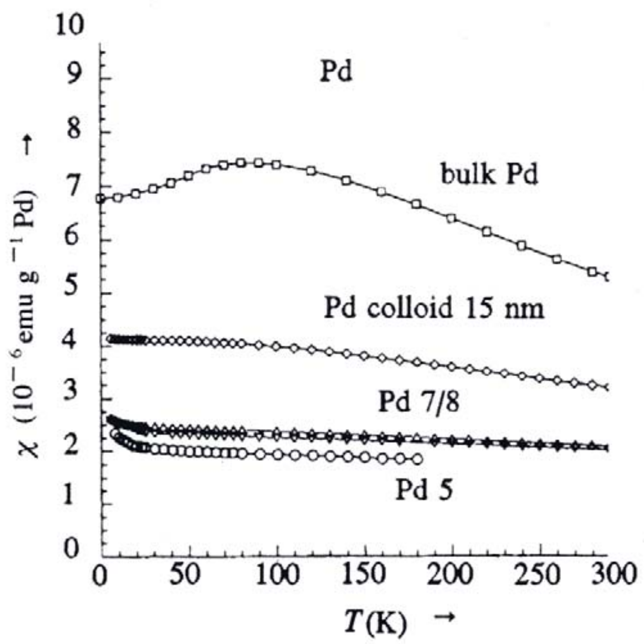

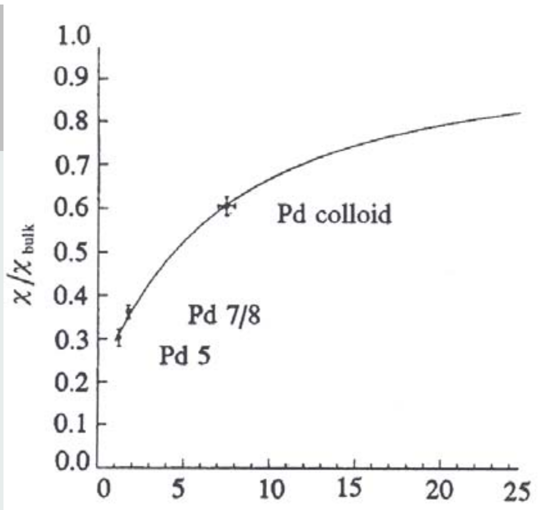

Figure 3-37. The susceptibility values of Pd5, Pd7/8 and 15 nm Pd colloids extrapolated to T = 0 and the best fit curve of the model describing the size dependence.

Figure 3-36. The temperature dependence of the susceptibility of various Pd particles compared to bulk palladium. The values are corrected for their diamagnetic contributions and normalized to the estimated weight of the Pd cores.

Cobalt –NRs - Selforganization

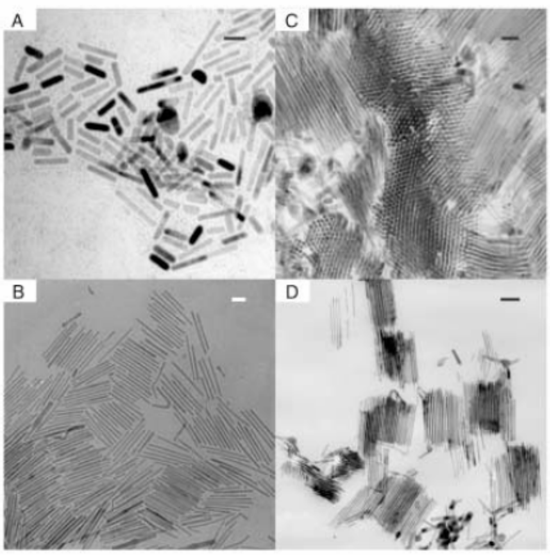

Figure 1. TEM micrographs of nanorods synthesized using hexadecylamine and A) octanoic acid (**2**), B) lauric acid (**1**), and C, D) stearic acid (**3**). The sample used in (C) was prepared by ultramicrotomy. Scale bar: 30 nm.

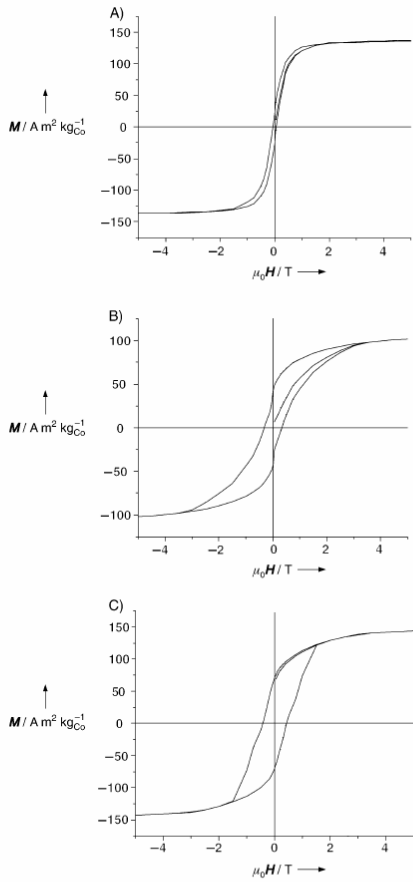

Figure 3. Magnetization curves recorded at 2 K of cobalt nanorods obtained in the presence of: A) HDA and octanoic acid (1:1) (**2**); B) HDA and lauric acid (1:1) (**1**); and C) HDA and stearic acid (1:1) (**3**).

Cobalt –QDot Arrays

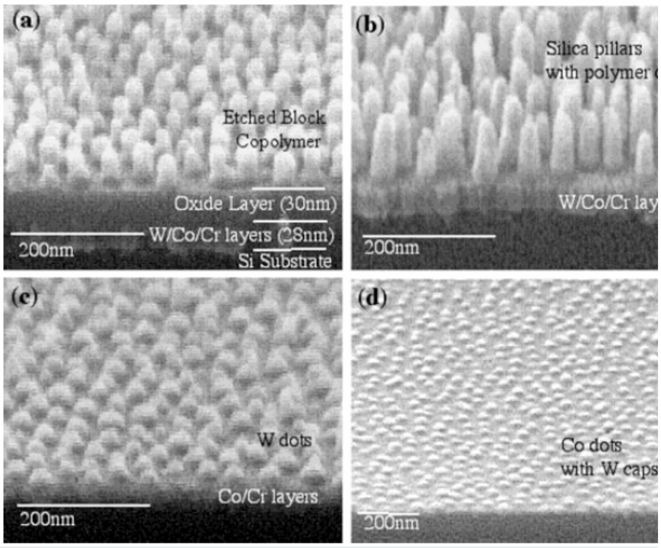

30Gdots per cm²

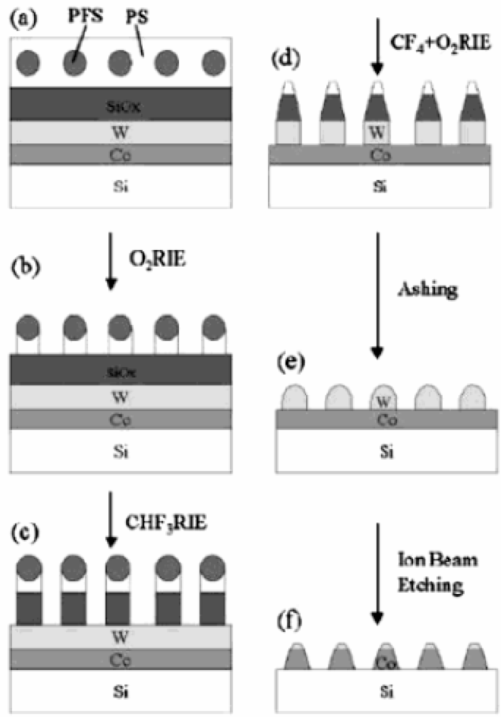

Fig. 2. Fabrication process of the cobalt dot array via block copolymer lithography. a) A block copolymer thin film on a multilayer of silica, tungsten, and cobalt. b) The block copolymer lithographic mask is formed through O_2-RIE process. The PFS domains are partly oxidized. c) The silica film is patterned using CHF_3-RIE. d) The tungsten hard mask is patterned using $CF_4 + O_2$-RIE. e) Removal of silica and residual polymer by high pressure CHF_3-RIE. f) The cobalt dot array is formed using ion beam etching.

Semiconductors

J. Am. Chem. Soc. 1990, 112, 1327–1332 1327

Nucleation and Growth of CdSe on ZnS Quantum Crystallite Seeds, and Vice Versa, in Inverse Micelle Media

A. R. Kortan, R. Hull, R. L. Opila, M. G. Bawendi, M. L. Steigerwald, P. J. Carroll, and L. E. Brus*

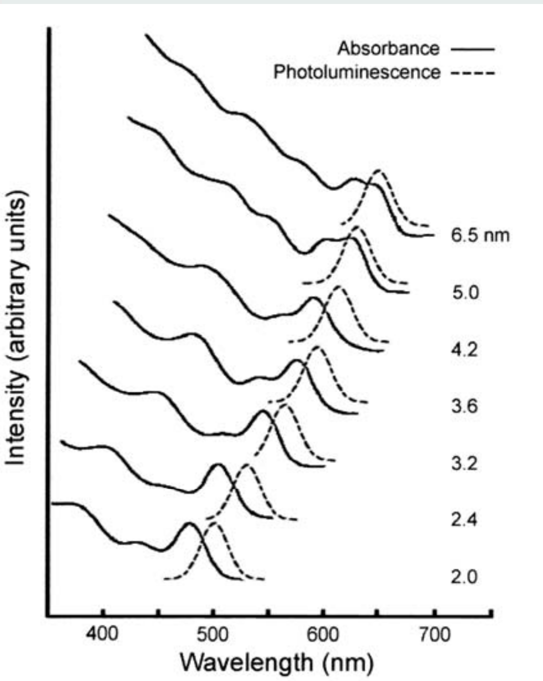

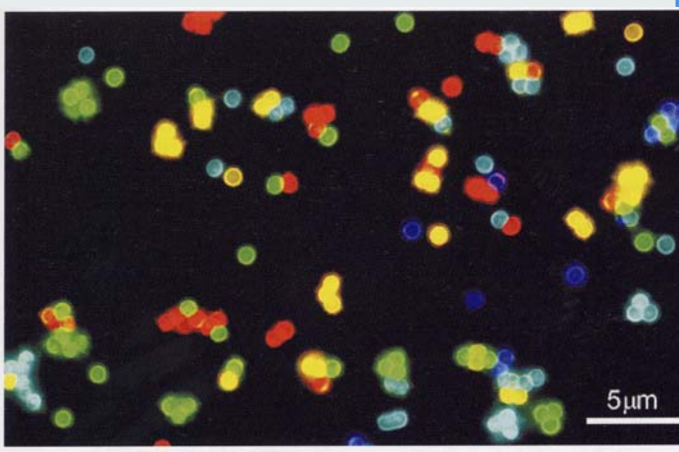

Fig. 12.5. Fluorescence micrograph of a mixture of CdSe/ZnS QD-tagged beads emitting single-color signals at 484, 508, 547, 575, and 611 nm. Reproduced with permission from [55].

Magnetic Q-Dots

R. NESPER ETH ZÜRICH & COLLEGIUM HELVETICUM

spin structures at the atomic level

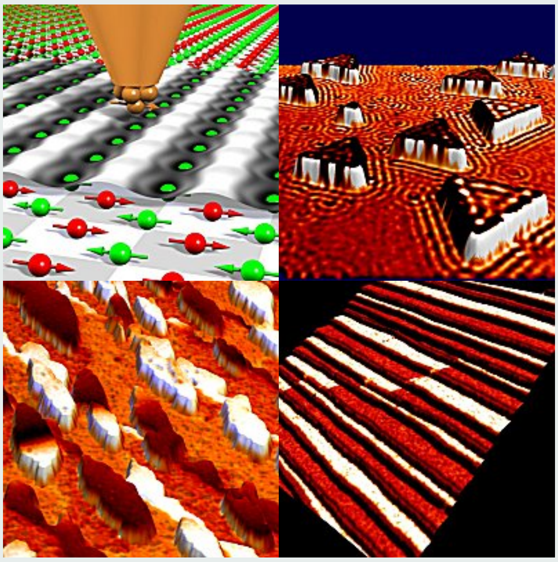

Structures at the Atomic Level

R. NESPER ETH ZÜRICH & COLLEGIUM HELVETICUM

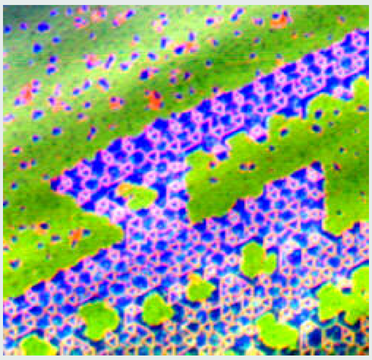

Reconstruction on terbium
The origin of this reconstruction are adsorbates (possibly CO) from an insufficient degassing process

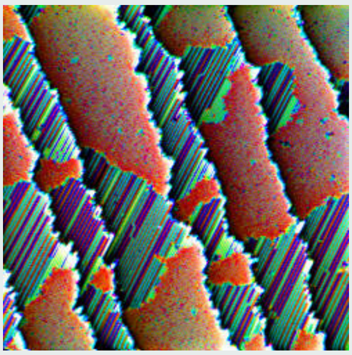

Tb on a W(110)
single crystal with thickness less than one single atomic layer. At this low coverage the Tb toms arrange in parallel lines, so- called superstructures", visible as stripes.

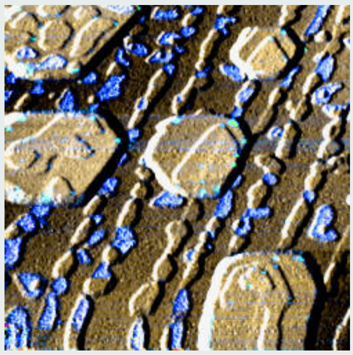

Gadolinium on W
Where the surface appears **blue, hydrogen** has been adsorbed on it changing the surface electronic structure drastically.

Electron States Mapped

In 3D electron systems we find simple **Bloch states** which are scattered at ionized dopants.

In **2D** much more complicated and much stronger standing wave pattern than in the 3D electron system.

1D systems containing one or two subbands have been found below charged step edges. Their local density of states shows nearly 100 % corrugation pointing to weakly localized states. Alignement with the disorder potential is directly observed.

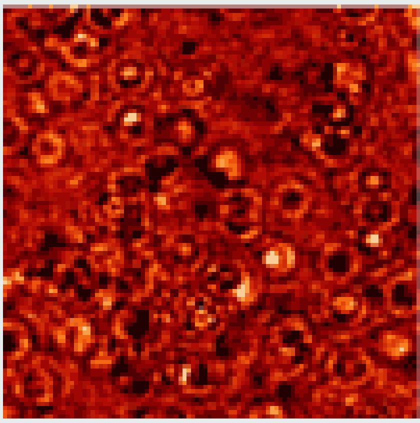

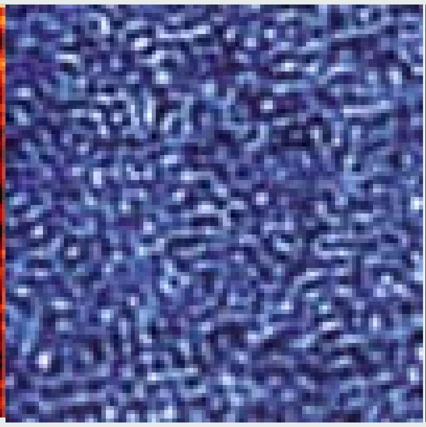

Surface Probe Gallery

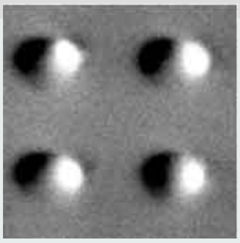

Switching behavior of single domain particles

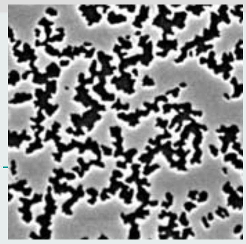

Magnetic Domains on CoPt-multilayers

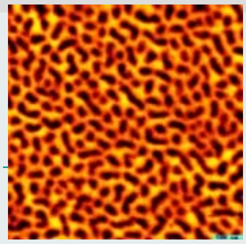

Domain growth on manganite perovskites

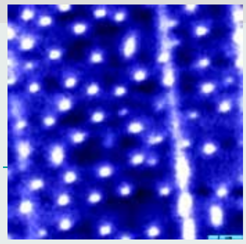

Vortices on High Tc Superconductors

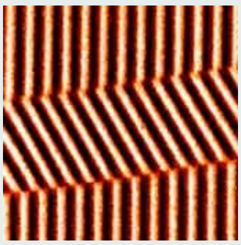

Investigation of magnetic bit structures

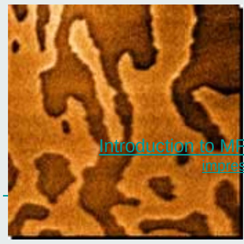

Reorientation transition of ultrathin cobalt films on Au(111)

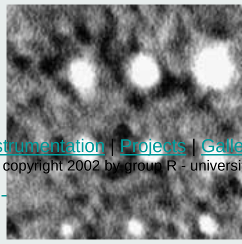

Domain writing with MFM on ultrathin cobalt films

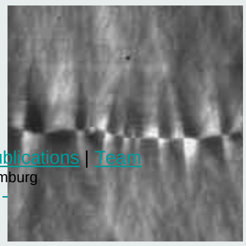

Domain walls and ripple structure of thin cobalt films

Semiconductors

CdSe Nanocrystal Rods/Poly(3-hexylthiophene) Composite Photovoltaic Devices**

By *Wendy U. Huynh, Xiaogang Peng,* and *A. Paul Alivisatos**

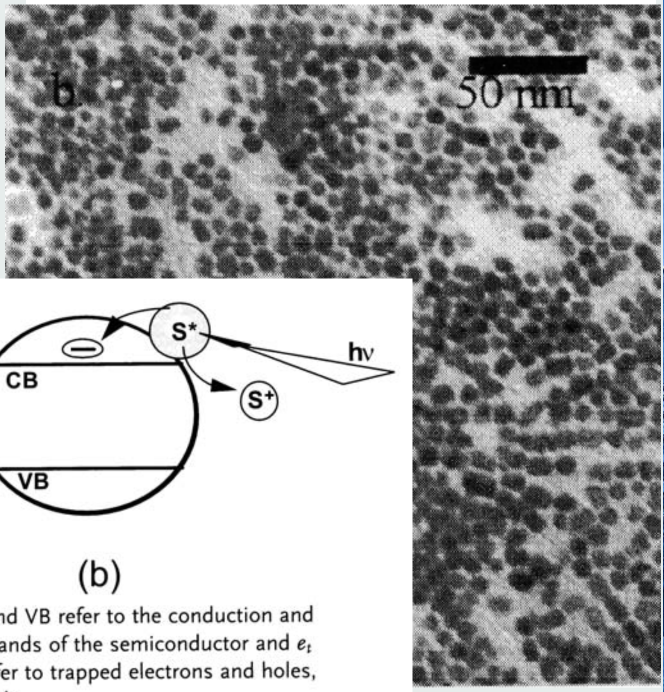

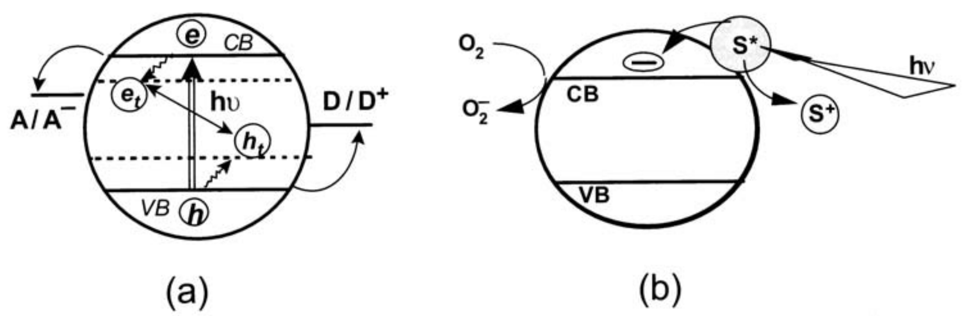

Fig. 19.1. Photoinduced charge transfer processes in semiconductor nanoclusters. (a) Under bandgap excitation and (b) sensitized charge injection by exciting adsorbed sensitizer (S). CB and VB refer to the conduction and valence bands of the semiconductor and e_t and h_t refer to trapped electrons and holes, respectively.

Semiconductors

J. Am. Chem. Soc. **1990**, *112*, 1327–1332 1327

Nucleation and Growth of CdSe on ZnS Quantum Crystallite Seeds, and Vice Versa, in Inverse Micelle Media

A. R. Kortan, R. Hull, R. L. Opila, M. G. Bawendi, M. L. Steigerwald, P. J. Carroll, and L. E. Brus*

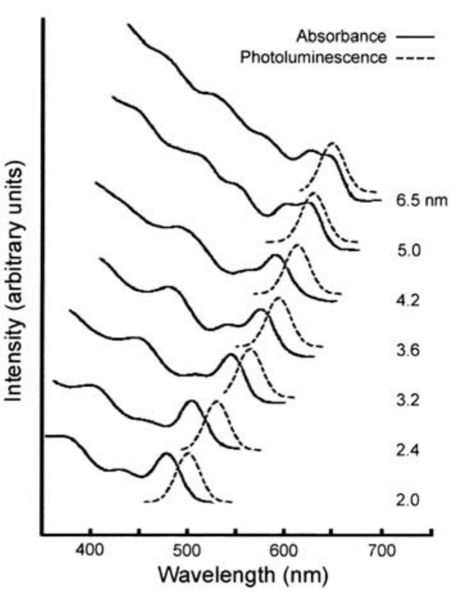

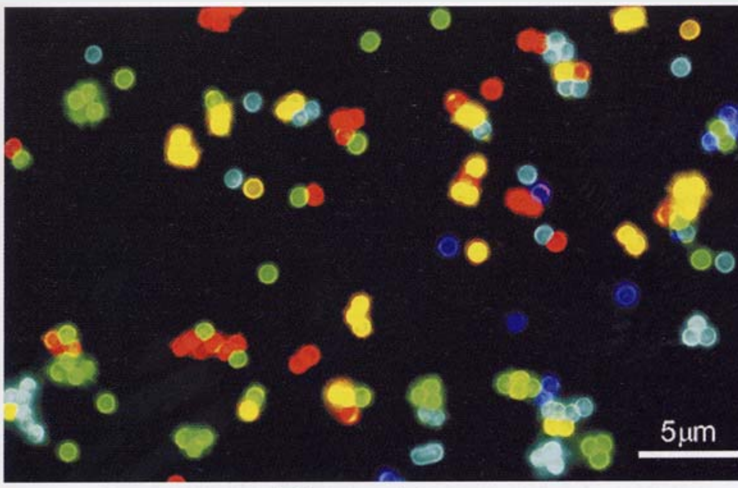

Fig. 12.5. Fluorescence micrograph of a mixture of CdSe/ZnS QD-tagged beads emitting single-color signals at 484, 508, 547, 575, and 611 nm. Reproduced with permission from [55].

Semiconductors

Wet Chemical Synthesis of Highly Luminescent HgTe/CdS Core/Shell Nanocrystals**

By *Mike T. Harrison, Steve V. Kershaw, Andrey L. Rogach, Andreas Kornowski, Alex Eychmüller,* and *Horst Weller**

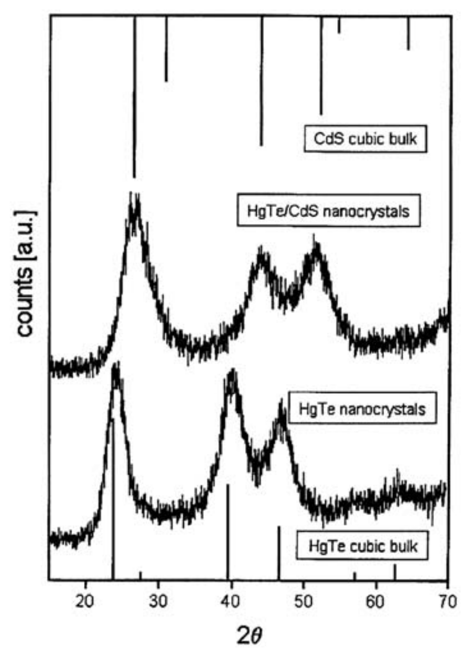

The starting nanocrystalline HgTe samples were prepared as follows: H_2Te gas, buffered in a slow nitrogen flow, was passed through a vigorously stirred N_2-saturated solution of 0.471 g $Hg(ClO_4)_2 \cdot 3H_2O$ (Alfa, 99.9 %) and 0.250 mL 1-thioglycerol (Fluka, ≥ 99 %) in 60 mL de-ionized water. The reaction was carried out in basic conditions by adjusting the pH to 10.0 using 1 M NaOH, and the H_2Te gas was generated in situ by the reaction of 20 mL 0.1 M H_2SO_4 with 49 mg Al_2Te_3. Thus, the molar ratio of $Hg^{2+}/RS^-/Te^{2-}$ was 1:2.88:0.32.

In order to attempt the growth of a layer of CdS on the bare organically capped HgTe nanocrystals, a 10 mL portion of the as-prepared HgTe solution was diluted down to 100 mL and 0.161 g $Cd(ClO_4)_2 \cdot 6H_2O$ (Alfa, 99.9 %) was added along with an extra 0.042 mL 1-thioglycerol. The pH was again adjusted to around 10, producing a slightly turbid solution. A 0.38 mmol portion of H_2S, either passed directly from a cylinder or generated in situ by the reaction of dilute H_2SO_4 with 30 mg Na_2S, was then injected into the vigorously stirred solution. The turbidity disappeared, resulting in a clear, golden-brown solution. Both the bare and capped solutions were then separately placed in flasks fitted with a reflux condenser and thermometer, and heated under an N_2 atmosphere with vigorous stirring to boiling point using a heating mantle. Aliquots were removed at various time intervals to monitor the effect of the heating process.

Chalcogenide Clusters in Chemical Compounds

D. Fenske et al.

$$2xMX + yPR_3 + xE(SiMe_3)_2 \xrightarrow[-\,2xSiMe_3X]{} [M_{2x}E_x(PR_3)_y]$$

M = Metall X = Halogen E = S, Se, Te R = organ. Gruppe

$Ag_{172}Se_{40}(Se\text{-}Bu)_{92}dppp_4$

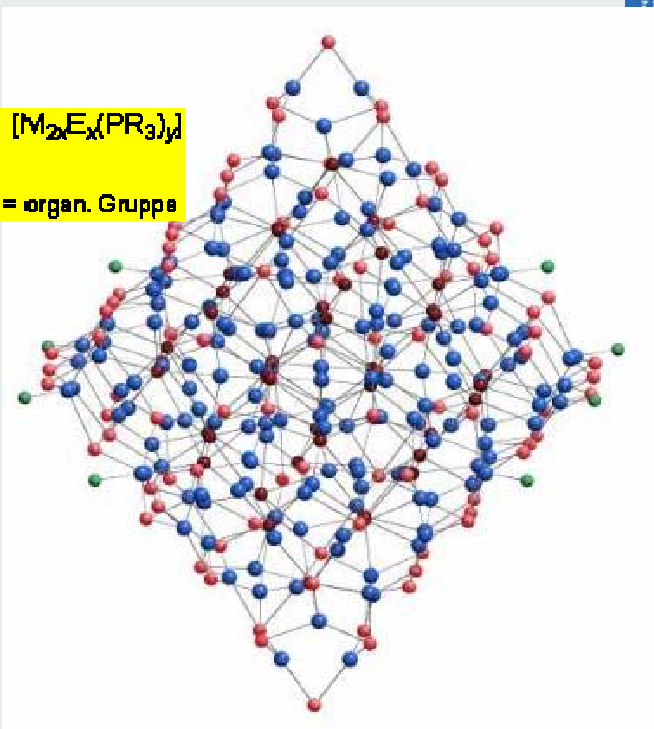

Huge Molecu

A. Müller et al.

Mo_{154}
Mo_{176}
Mo_{248}

$[\{Mo_{128}Eu_4O_{388}H_{10}(H_2O)_{81}\}]^{20-}$

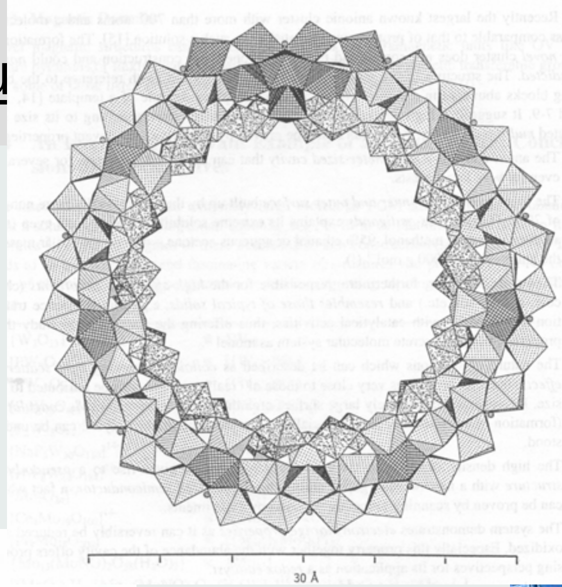

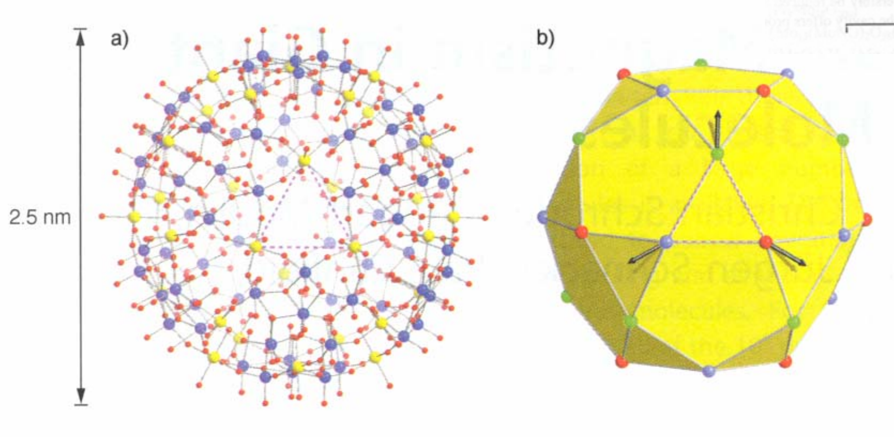

Huge Molecules

A. Müller et al.

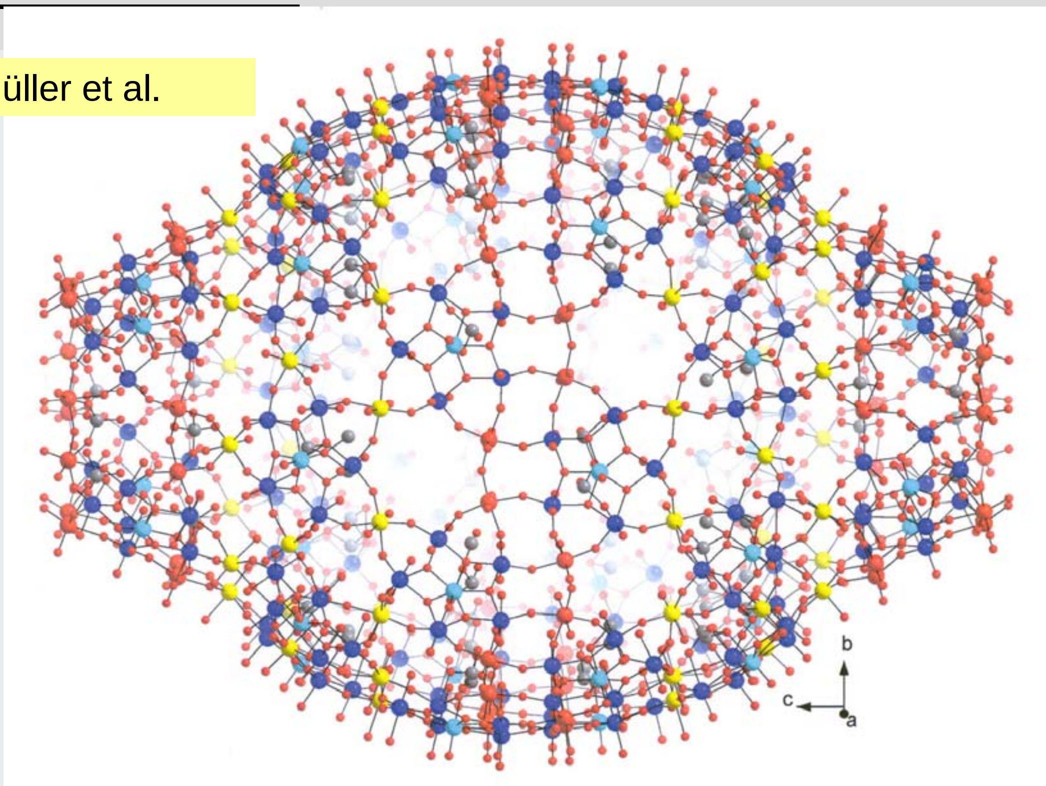

Huge Molecules

A. Müller et al.

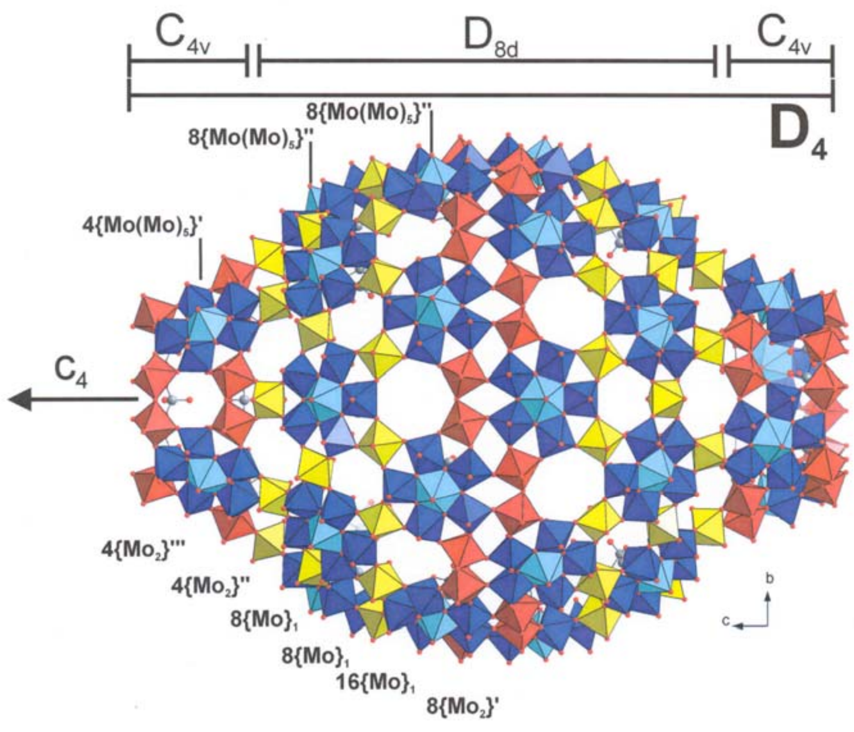

Huge Molecules

A. Müller et al.

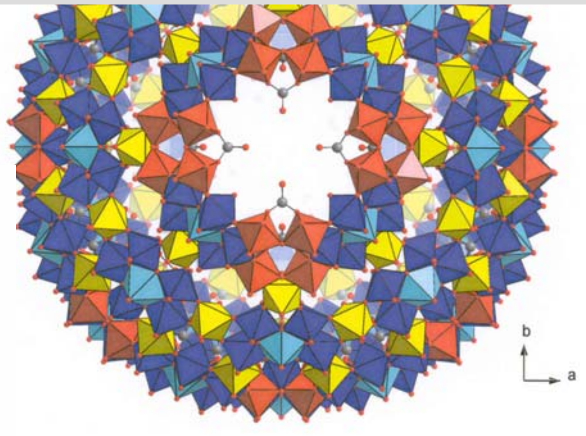

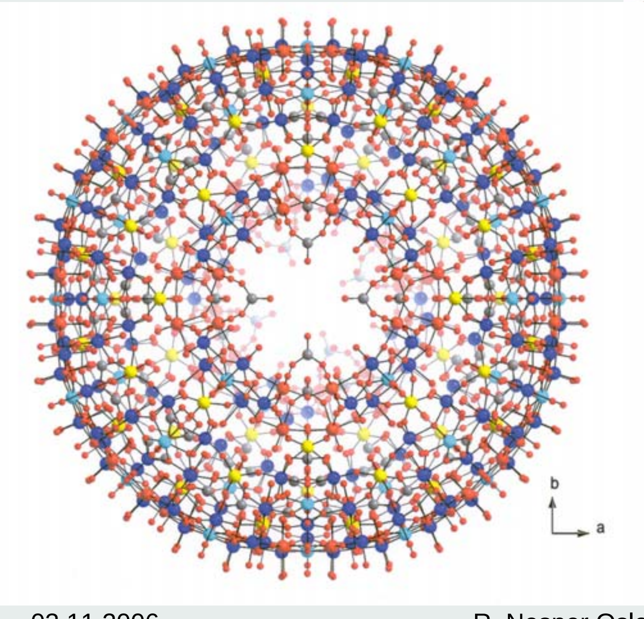

Assembly of Huge Molecules

A. Müller, E. Diemann,
Nature

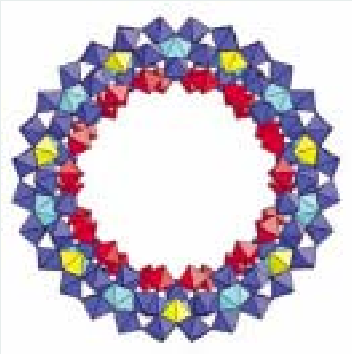

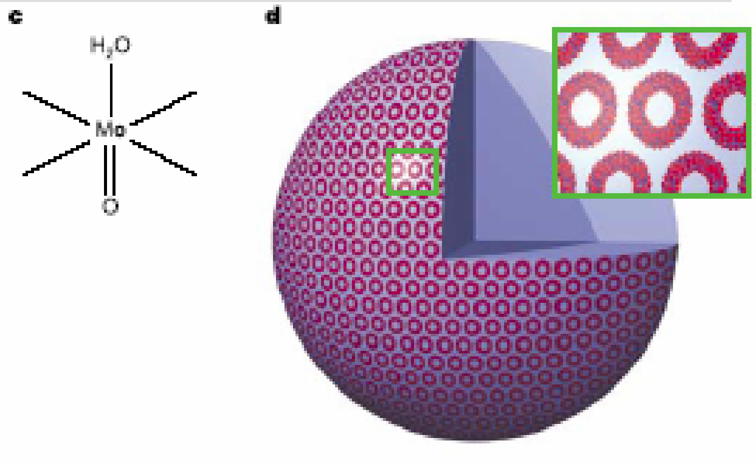

Figure 1 Structure of the 3.6mm size {Mo154}-type nanowheel with a hydrophilic surface and nanosized central cavity. a, Space-filling representation (blue and light blue, Mo atoms; red, O atoms). b, Polyhedral representation, demonstrating the abundance of pentagonal (Mo)Mo5 units (in blue) probably influencing the water structure (Mo2 units in red, Mo1 units in yellow). c, The typical smallest fragment with a metal atom and its coordination sphere, that is, with one of the 70 H2O ligands causing the extreme hydrophilic nature that is responsible for the interaction with solvents such as water. d, Schematic plot of the vesicle structure formed from nanowheels (,45 nm radius) in aqueous solution, with inset showing enlarged nanowheels.